








Short-range organization and photophysical properties of CdSe quantum dots coupled with aryleneethynylenes

Christoph P Theurer¹, Antonia Weber¹ , Martin Richter²,
Markus Bender^{3,4}, Patrick Michel⁵, Debkumar Rana^{2,4} , Krishan Kumar⁵,
Uwe Bunz^{3,4} , Marcus Scheele^{5,6} , Petra Tegeder^{2,4} ,
Frank Schreiber^{1,6,*}  and Katharina Broch^{1,6,*} 

¹ Institut für Angewandte Physik, Universität Tübingen, Auf der Morgenstelle 10, D-72076 Tübingen, Germany

² Physikalisch-Chemisches Institut, Universität Heidelberg, Im Neuenheimer Feld 253/229, D-69120 Heidelberg, Germany

³ Organisch-Chemisches Institut, Universität Heidelberg, Im Neuenheimer Feld 270, D-69120 Heidelberg, Germany

⁴ Centre for Advanced Materials, Universität Heidelberg, Im Neuenheimer Feld 225, D-69120 Heidelberg, Germany

⁵ Institut für Physikalische und Theoretische Chemie, Universität Tübingen, Auf der Morgenstelle 18, D-72076 Tübingen, Germany

⁶ Center for Light-Matter Interactions, Sensors & Analytics (LISA⁺), Universität Tübingen, Auf der Morgenstelle 15, D-72076 Tübingen, Germany

E-mail: frank.schreiber@uni-tuebingen.de and brochkatharina@gmail.com

Received 30 November 2021, revised 28 January 2022

Accepted for publication 8 February 2022

Published 17 March 2022



Abstract

Hybrid organic–inorganic nanomaterials composed of organic semiconductors and inorganic quantum dots (QDs) are promising candidates for opto-electronic devices in a sustainable internet of things. Especially their ability to combine the advantages of both compounds in one material with new functionality, the energy-efficient production possibility and the applicability in thin films with little resource consumption are key benefits of these materials. However, a major challenge one is facing for these hybrid materials is the lack of a detailed understanding of the organic–inorganic interface which hampers the widespread application in devices. We advance the understanding of this interface by studying the short-range organization and binding motif of aryleneethynylenes coupled to CdSe QDs as an example system with various experimental methods. Clear evidence for an incorporation of the organic ligands in between the inorganic QDs is found, and polarization-modulation infrared reflection-absorption spectroscopy is shown to be a powerful technique to directly detect the binding in such hybrid thin-film systems. A monodentate binding and a connection of neighboring QDs by the aryleneethynylene molecules is identified. Using steady-state and time resolved spectroscopy, we further investigated the photophysics of these hybrid systems. Different passivation capabilities resulting in different decay dynamics of the QDs turned out to be the main influence of the ligands on the photophysics.

Supplementary material for this article is available [online](#)

Keywords: spectroscopy, quantum dots, organic semiconductors, organic–inorganic interface

(Some figures may appear in colour only in the online journal)

* Authors to whom any correspondence should be addressed.

1. Introduction

The internet of things is rapidly evolving and growing and new, functional materials with cost- and energy-efficient production procedures are highly desirable. One important step already taken in this evolution was the development and commercial launch of organic electronic devices, since they satisfy the low cost demands [1], but their functionality limits their application to certain fields [2]. Another promising material class is based on quantum dots (QD), which show exceptional, tunable optical properties and can be synthesized by cost-efficient bottom-up approaches [3]. While the two fields of organic electronics and QD-based devices are in themselves rapidly growing, a new field evolves between them, which is concerned with the combination of organic and inorganic compounds into one functional material. These hybrid organic–inorganic materials received increasing attention during the last years due to the fact that the advantages of both classes can be exploited [4, 5]. Since they can furthermore be produced with low energy effort and are applicable in thin films with little material consumption, they hold great promise for a sustainable internet of things [6–8]. Hybrid organic–inorganic materials are for example powerful candidates for optical communication [9], spin memory [5] and photon upconversion applications [10] as well as for solar cells with increased efficiency [11]. For all these applications, the organic–inorganic interface and charge and energy transfer processes through it are of key relevance [5, 11]. However, a clear picture of the interface, the structural arrangement and the chemical interactions is mostly missing and represents one major challenge for the further development of hybrid organic–inorganic nanostructures [5].

With this study, we aim to contribute to the understanding of the organic–inorganic interface and provide compelling evidence of direct binding of carboxylate groups of aryleneethynylene (AE) derivatives to CdSe QDs. We chose these promising systems due to the reported fluorescence variations and the suggested energy transfer in hybrid films of sodium 2,2',2'',2''',2''',2''''',2''''',2''''''-(((benzene-1,2,4,5-tetrayltetrakis(ethyne-2,1-diyl))tetrakis(benzene-4,1-diyl))tetrakis(azanetriyl))octaacetate (AE 1, see figure 1) and CdSe QDs in [12]. A comparison to samples containing sodium 2, 2',2'',2'''-(((2,5-bis((E)-4-methoxystyryl)-1,4-phenylene)bis(ethyne-2,1-diyl))-bis(4,1-phenylene))-(azanetriyl))tetraacetate (AE 2, see figure 1) and CdSe QDs allows us to analyze the impact of different substitutions, resulting in a changed number of carboxylate groups and changed electronic properties while keeping the structure similar. With grazing-incidence small angle x-ray scattering (GISAXS) measurements the short-range organization in these complex systems was investigated and the incorporation of the AEs in between the QDs was observed. By photoluminescence and vibrational spectroscopy a binding of the AEs to the QDs is shown, creating a connection of neighboring QDs. In particular polarization-modulation infrared reflection-absorption spectroscopy (PMIRRAS) is established as a powerful tool to characterize the binding motif, which should be also applicable to other hybrid

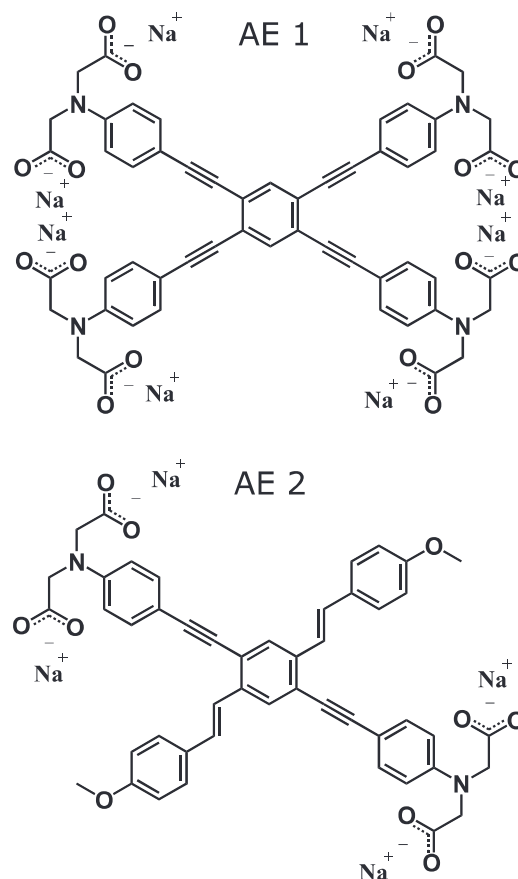


Figure 1. Chemical structure of the aryleneethynylene derivatives AE 1 and AE 2.

systems, e.g. with environmentally friendly QDs [13]. Interestingly, despite the chemical binding, no indications for charge or energy transfer between the AEs and the QDs in both systems are found by ultrafast transient absorption (TA) spectroscopy. Instead, it is found that the photophysics are dominated by differences in the surface passivation of the QDs due to the different ligands.

2. Experimental methods

2.1. Material synthesis

The synthesis of the CdSe QDs with a diameter of ~ 5.4 nm dispersed in hexane and stabilized by hexadecylamine, trioctylphosphineoxide (TOPO) and oleic acid (CdSe/nat) is described in [12] and is based on [14]. The ligand-exchange procedure yielding iodide stabilized QDs (CdSe/I[−]) in n-methylformamide (NMF) as well as the synthesis of the sodium 2,2',2'',2''',2''',2''''',2''''',2''''''-(((benzene-1,2,4,5-tetrayltetrakis(ethyne-2,1-diyl))tetrakis(benzene-4,1-diyl))tetrakis(azanetriyl))octaacetate (AE 1, see figure 1) are also described therein [12, 14].

Sodium 2, 2', 2'', 2'''-(((2,5-bis((E)-4-methoxystyryl)-1,4-phenylene)bis(ethyne-2,1-diyl))-bis(4,1-phenylene))bis(azanetriyl))tetraacetate (AE 2, see figure 1):

AE 2-COOEt (400 mg, 436 μ mol) was dissolved in MeOH/H₂O (1:1, 10 ml/10 ml) and NaOH (698 mg, 17.5 mmol)

was added. The resulting mixture was stirred at 70 °C for 2 d. The solvent was evaporated in vacuum. The residue was dissolved in H₂O and filtrated. The resulting solution was adjusted to pH 7 and dialyzed against DI H₂O for 5 d. After filtration and freeze-drying the title compound AE 2 was afforded as yellow solid (344 mg, 98%). ¹H NMR (600 MHz, D₂O): δ = 7.95–7.914 (m, 6 H), 6.87–6.84 (m, 4 H), 6.74–6.70 (m, 10 H), 4.15–4.13 (m, 14 H) ppm. Due to low solubility, the ¹³C NMR spectrum could not be obtained. IR (cm⁻¹): ν = 3668, 3650, 3304, 3018, 2924, 2357, 2341, 2327, 2188, 1997, 1663, 1602, 1538, 1510, 1461, 1429, 1382, 1334, 1293, 1271, 1245, 1202, 1173, 1114, 1051, 1027, 987, 957, 903, 872, 818, 750, 668, 651, 646, 631, 605, 589, 558, 555, 524, 468.

The precursors of AE 2 and their synthesis are reported in the supporting information (available online at stacks.iop.org/NANO/33/230001/mmedia).

2.2. Thin-film preparation

All samples were prepared from the liquid phase in a nitrogen filled glovebox. For the neat AE films around 50 μ l of the respective AE in NMF ($\sim 2 \times 10^{-4}$ mol l⁻¹) were dropped onto the substrate, left undisturbed for at least 1 h and annealed at 110 °C for 1 h afterwards. We chose an annealing temperature of 110 °C and a duration of 1 h to effectively remove the NMF from the sample while conserving the AEs and avoiding too fast evaporation which can induce additional defects in the sample. The thickness of the resulting films was 20–60 nm, as determined by profilometer measurements, see the supporting information for details. The films of the CdSe QDs with their native ligands hexadecylamine, TOPO and oleic acid in hexane ($\sim 7 \times 10^{-6}$ mol l⁻¹) were prepared in the same manner.

To prepare thin films of the iodide-capped CdSe QDs, the dispersion in NMF ($\sim 1.4 \times 10^{-4}$ mol l⁻¹) was dropped onto a tilted substrate. By the droplet gliding down on the substrate, a thin film was formed. After at least 1 h, the samples were annealed for another hour at 110 °C. The CdSe/I⁻ and CdSe/nat films have thicknesses in the range of 180 nm to 330 nm. For the mixed films (CdSe/I⁻/AE) ~ 50 μ l of the respective AE solution and ~ 35 μ l of the 1:9 diluted iodide-capped CdSe QD solution were dropped onto the substrate and left undisturbed for at least 1 h. After drying the sample at 110 °C on a hotplate it was washed 3 times with NMF to remove unbound AEs and finally annealed for 1 h at 110 °C, yielding 130–290 nm thick films.

2.3. Characterization

The steady-state UV–vis absorption was measured with a Perkin Elmer Lambda 950 UV–vis–NIR spectrometer. The photoluminescence spectra were taken with a Horiba Jobin Yvon LabRAM HR spectrometer, equipped with a 50 \times objective and an excitation laser with a wavelength of 532 nm. The UV–vis absorption and photoluminescence measurements were done on 150 μ m thick borosilicate glass slides as substrates. To prevent oxidation or photo-degradation of the samples they were sealed by a second glass in nitrogen atmosphere. The same samples were used for

transient absorption (TA) measurements on a commercially available pump-probe setup (HELIOS from Ultrafast Systems). Details can be found in [15]. In short, the fundamental beam of a Ti:Sa amplified laser system (Astrella, Coherent, 4kHz), with a center wavelength of 800 nm was used to pump an optical parametric amplifier (TOPAS Prime, Light Conversion). With the optical parametric amplifier pump pulses with choosable wavelengths can be generated while broad band probe pulses were generated in sapphire. Magic angle polarization between the pump and the probe pulse was used for all measurements. The measurements with 620 nm wavelength excitation were done with low excitation densities (<0.37 electron–hole pairs per QD) to prevent many-particle interactions. Additional measurements with <0.1 electron–hole pairs per QD showed similar dynamics. The measurements with a pump wavelength of 350 nm were done with one common excitation intensity for all samples to ensure comparability between them. The weak TA signal of the neat AE films required to choose a comparably high intensity, resulting in ~ 1.2 electron–hole pairs per QD for the QD-containing samples. Reference measurements on the neat QD samples with 1/10 of this intensity resulted in slower decay dynamics. The determination of the excitation density is detailed in the supporting information.

Grazing-incidence small angle x-ray scattering (GISAXS) experiments were done in vacuum to prevent oxidation. A Xeuss 2.0, (Xenocs) laboratory instrument equipped with a microfocus x-ray source ($\lambda = 1.541$ Å) and a Pilatus 300k detector was used. The infrared spectra were taken with a Vertex 70 (Bruker) Fourier transform infrared (FTIR) spectrometer in transmission mode on doubly polished silicon substrates. Polarization-modulation infrared reflection-absorption spectroscopy (PMIRRAS) experiments were performed on the PMA 50 unit of the same spectrometer under an incidence angle of 80° with a resolution of 4 cm⁻¹ and a half-wave retardation of 1500 cm⁻¹. Gold-coated silicon wafers were used as substrates, 1000 scans were averaged per spectrum and the measurement chamber was flushed with nitrogen.

3. Results

3.1. Vibrational spectroscopy

To demonstrate their presence and clarify the nature of organic linkers in coupled organic–inorganic systems, Raman spectroscopy or infrared vibrational spectroscopy are widely used in the literature [12, 16, 17]. FTIR spectra of the samples investigated in this study are shown in figure 2(a). The spectra of the sample of CdSe QDs covered by their native ligands (CdSe/nat) and the sample of the iodide stabilized QDs (CdSe/I⁻) are dominated by contributions from water vapor (between 1300 cm⁻¹ and 2000 cm⁻¹) and carbon dioxide (around 2350 cm⁻¹), but for the former, C–H stretching vibrations of the native ligands above 2800 cm⁻¹ are clearly observed. In contrast, the spectra of the AE films show characteristic vibrational peaks from 1150 cm⁻¹ to 1750 cm⁻¹ and a weak peak at 2195 cm⁻¹. The latter is

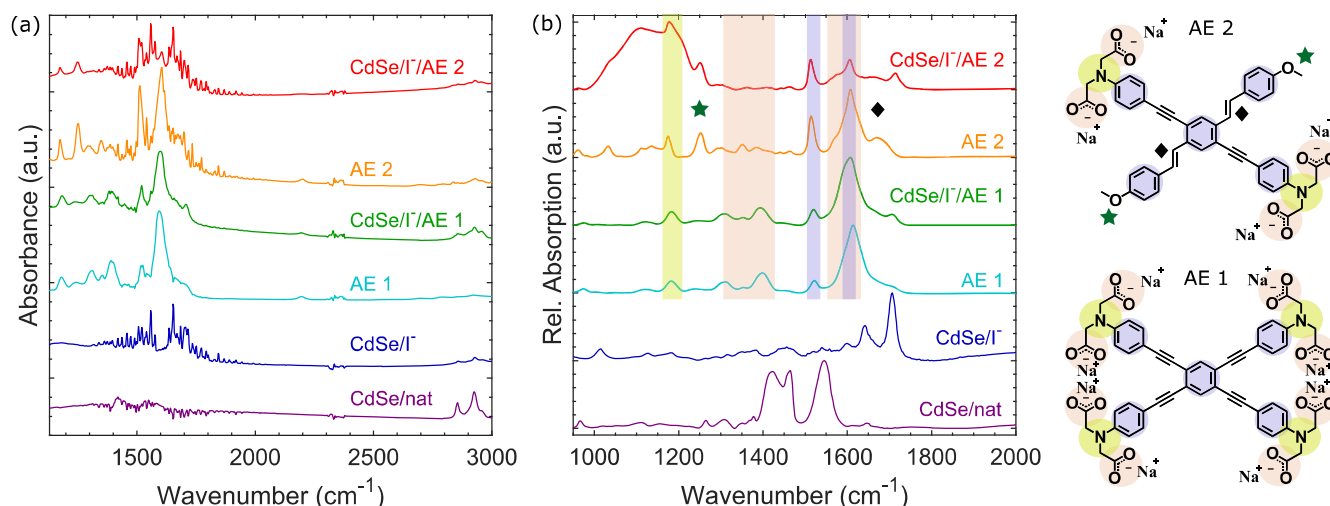


Figure 2. Vibrational spectroscopy of the CdSe/I[−]/AE films and the reference films: (a) FTIR spectra, (b) PMIRRAS spectra. In (b) the spectral regions of the characteristic vibrations of the groups marked on the molecular structures on the right are indicated. For the spectrum of the AE 2 film the peak assigned to a C=C stretching mode is additionally marked by a black diamond and the peak assigned to an alkyl aryl ether C–O stretching mode by a green star.

assigned to the characteristic C≡C stretching vibration of the alkyne moieties [18], and the main peak around 1600 cm^{−1} is in the region of carboxylate and aromatic ring stretch vibrations, which are both present in both AEs. The peaks of the AEs dominate the FTIR spectra of the CdSe/I[−]/AE films which is clear evidence for the successful addition of both AEs to the system. However, the exact organization and a potential binding of the AEs to the QDs cannot be conclusively deduced from FTIR spectroscopy in transmission mode. Hence, PMIRRAS spectroscopy was used as an additional technique with high sensitivity, high resolution and low noise level [19, 20]. PMIRRAS spectra of the region with the dominant peaks of the AEs are shown in figure 2(b). For the CdSe/nat film characteristic peaks at 1545 cm^{−1}, 1464 cm^{−1} and 1421 cm^{−1} are observed, which match the peak positions of vibrational spectra of TOPO and oleate-capped CdSe QDs [21]. In the spectrum of the CdSe/I[−] film these peaks are missing which indicates, together with the almost complete absence of the C–H stretching vibrations in figure 2(a), the successful removal of the native ligands. Instead, new peaks at 1706 cm^{−1}, 1642 cm^{−1}, 1600 cm^{−1}, and 1014 cm^{−1} appear, which resemble the peaks reported in [14] for iodide-capped CdSe QDs and could stem from remaining NMF in this sample [22]. It is noted that a second annealing cycle at 190 °C for 1 h does not change the spectrum. The spectra of the AE and the CdSe/I[−]/AE films will be analyzed and compared in more detail in the following to get insights into the binding behavior. The characteristic peaks associated with specific molecular groups are color-coded and marked on the right of figure 2(b) in the molecular structures.

We start with the spectrum of the neat AE 1 film. AE 1 is a highly symmetric molecule and its PMIRRAS spectrum exhibits relatively few, well-resolved peaks at 1614 cm^{−1}, 1522 cm^{−1}, 1398 cm^{−1}, 1311 cm^{−1}, 1182 cm^{−1}, and 974 cm^{−1}. The strongest one at 1614 cm^{−1} lies at a position where aromatic ring stretching and carboxylate vibrations are

expected and is most likely a superposition of both [18, 23]. The sharp peak at 1522 cm^{−1} is furthermore assigned to aromatic ring stretch vibrations [18] while the peaks at 1398 cm^{−1} and 1311 cm^{−1} are assigned to carboxylate vibrations [18, 23]. The peak at 1182 cm^{−1} perfectly matches the position of the tertiary amino C–N stretching mode and the smaller peaks at lower wavenumbers can be assigned to aromatic C–H in-plane bending modes [18]. The PMIRRAS spectrum of the CdSe/I[−]/AE 1 film is clearly dominated by the mentioned peaks of the AE 1 vibrations and resembles the spectrum of the AE 1 film, although with some significant changes. At 1707 cm^{−1} a peak is observable in the spectrum of the CdSe/I[−]/AE 1 film while in the neat AE 1 film only a weak shoulder is visible around this wavenumber. The main peak in the spectrum of the CdSe/I[−]/AE 1 sample is slightly shifted to 1607 cm^{−1} compared to the spectrum of the AE 1 film and additionally exhibits a shoulder towards smaller wavenumbers. In contrast, the sharp peaks correlated with the aromatic ring stretching mode at 1520 cm^{−1} and the tertiary amino C–N stretching mode at 1184 cm^{−1} remain almost unchanged.

A comparable PMIRRAS spectrum was also obtained for the neat AE 2 film. The main peak is located at 1607 cm^{−1}, again in the range of aromatic ring stretching and carboxylate modes. The sharp peaks of the aromatic ring stretching mode at 1513 cm^{−1} and of the tertiary amino group at 1175 cm^{−1} are also clearly resolved. Smaller peaks between 1300 cm^{−1} and 1400 cm^{−1} are again assigned to carboxylate vibrations and the peaks below 1150 cm^{−1} are assigned to C–H bending modes. In addition to the aforementioned peaks, a broader peak around 1670 cm^{−1} is visible that can be assigned to a C=C stretching mode of the alkene moieties (marked by black diamonds in figure 2(b)). Furthermore, there is a sharp peak at 1252 cm^{−1}, at the position of the alkyl aryl ether C–O stretching mode (marked by a green star). Comparing the spectrum of the CdSe/I[−]/AE 2 film to the spectrum of the AE 2 film, stronger differences than for the AE 1 system are

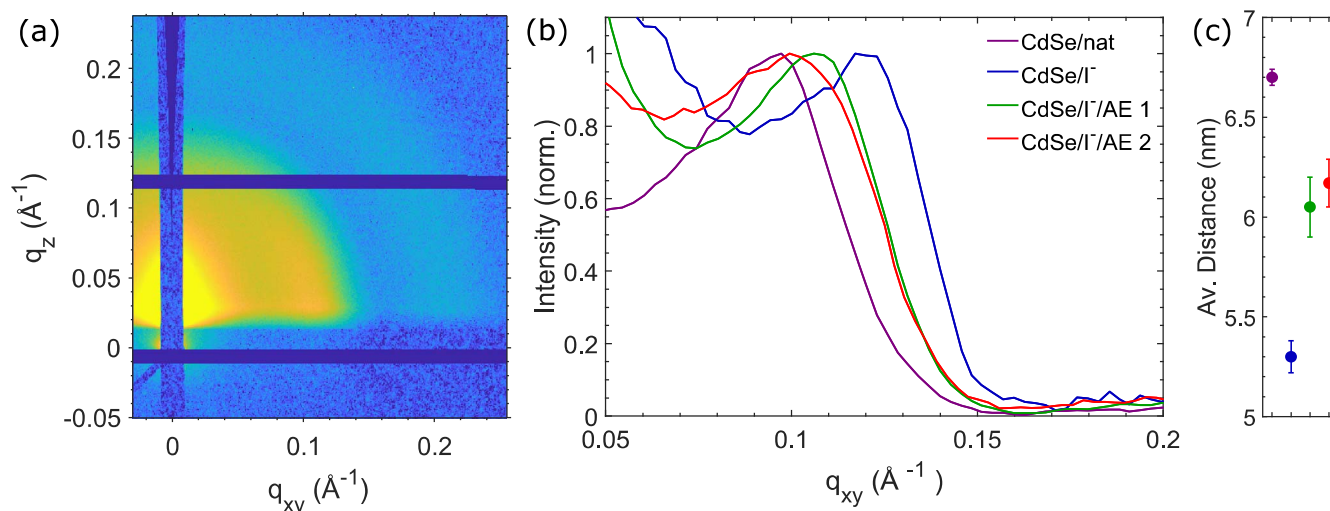


Figure 3. GISAXS structure analysis. (a) Reciprocal space map of a CdSe/I[−]/AE 1 film, (b) integrated intensity ($0.02 \text{ \AA}^{-1} < q_z < 0.03 \text{ \AA}^{-1}$) as function of the in-plane scattering vector q_{xy} , (c) average distance between the centers of the CdSe QDs derived from the peak positions in (b) using the same color code. The error bars are derived from variations between several samples.

Table 1. Summary of the main vibrational peaks of the samples containing AEs and their assigned functional groups, compare figure 2(b). Vibrational frequencies given in cm^{-1} .

	AE 1	CdSe/I [−] /AE 1	AE 2	CdSe/I [−] /AE 2
Carboxylate	1614, 1398, 1311	1607, 1394, 1310	1607, 1300–1400	1606
Aromatic ring	1614, 1522	1607, 1520	1607, 1513	1606, 1513
Tertiary amino	1182	1184	1175	1177
Aromatic C–H	<1150	<1150	<1150	<1150
Alkene C=C			1670	1665
Alkyl aryl ether			1252	1251
Carbonyl		1707		1714
Ether C–O–Cd				1130

apparent. First, the peak at 1606 cm^{-1} is much weaker in the CdSe/I[−]/AE 2 film and instead a very broad peak around 1130 cm^{-1} dominates the spectrum. Second, the weak peaks found in the spectrum of the AE 2 sample between 1300 cm^{-1} and 1400 cm^{-1} disappear almost completely and third, a sharp peak arises at 1714 cm^{-1} , which is not present in the spectrum of the neat AE 2 film. The sharp peaks at 1513 cm^{-1} , 1251 cm^{-1} and 1177 cm^{-1} , assigned to aromatic ring stretching, alkyl aryl ether stretching and tertiary amino group modes, however, remain nearly unchanged. In summary, the vibrational spectroscopy data proof the presence of both AEs in the systems, and the PMIRRAS technique allows to observe changes between some peaks of the spectra of the neat AE films and the CdSe/I[−]/AE films, which will be discussed later. The main observed peaks and their assigned functional groups are summarized in table 1.

3.2. X-ray scattering

To investigate the impact of the AEs on the structure formation of the CdSe/I[−]/AE films in comparison to the CdSe/nat and CdSe/I[−] films, GISAXS measurement on glass, silicon and gold-coated substrates were conducted [24]. The general appearance of the reciprocal space maps of all

samples is similar and a representative one of a CdSe/I[−]/AE 1 film is shown in figure 3(a). It exhibits a broad scattering ring at approximately $q = 0.1 \text{ \AA}^{-1}$ and a second, much weaker one at approximately twice this value. These rings result from constructive interference between neighboring QDs, but sharp Bragg peaks are missing. Thus, the reciprocal space maps indicate a lack of long-range in- and out-of-plane order, but the existence of some short range (in-plane) order with a distinct average distance between neighboring QDs. We note that for less complex coupled organic–inorganic nanostructures pronounced long-range order has been reported before [25, 26]. In figure 3(b) horizontal line cuts along q_{xy} , integrated over $0.02 \text{ \AA}^{-1} < q_z < 0.03 \text{ \AA}^{-1}$, are shown. A clear difference in peak position between the CdSe/nat, the CdSe/I[−] and the two systems with AEs is obtained. This peak position is converted to an average center-to-center distance of neighboring QDs in the respective samples, which is displayed in figure 3(c). For the CdSe/I[−] film the average distance of 5.3 nm matches the average diameter of the CdSe QD core (determined by UV–vis spectroscopy, see supporting information), implying direct contact between adjacent QDs. The films of CdSe QDs with the native ligands hexadecylamine, TOPO and oleic acid have average distances of 6.7 nm . The resulting gap of 1.4 nm between two QDs fits

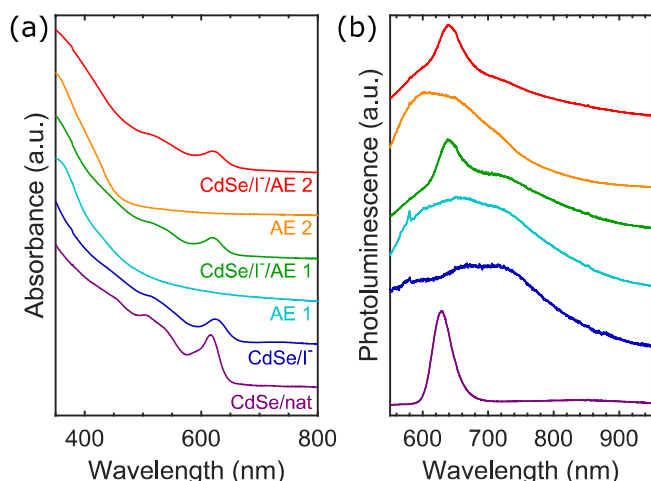


Figure 4. (a) UV-vis absorption spectra and (b) photoluminescence spectra, excited at 532 nm. The spectra are vertically offset for clarity and in the same color code.

with reports of oleic acid-capped QDs [27]. For the CdSe/I[−]/AE films, the average distances of neighboring QDs are in between the two mentioned ones, with 6.1 nm and 6.2 nm for AE 1 and AE 2, respectively. Hence, a gap of 0.8 nm and 0.9 nm between two QDs is formed which would fit with the size of one incorporated AE that connects the two QDs.

Optical spectroscopy

How the combination of the inorganic CdSe QDs and the organic AEs into one system influences the optical response of the two compounds was studied by UV-vis absorption (figure 4(a)) and photoluminescence (figure 4(b)) spectroscopy. The absorption spectrum of the CdSe/nat film shows the typical sharp 1S(e)-1S_{3/2}(h) transition at 616 nm and the 1S(e)-2S_{3/2}(h), 1P(e)-1P_{3/2}(h) and 1S(e)-3S_{1/2}(h) transitions at smaller wavelengths [28–30]. The absorption spectrum of the CdSe/I[−] film looks very similar, but is slightly red-shifted and broadened due to the changed polarizability of the environment. The two neat AE films exhibit a broad absorption at small wavelengths, probably due to different rotamers [31], and the absorption spectra of the CdSe/I[−]/AE films can be well described by a superposition of the spectrum of the respective AE sample and the spectrum of the CdSe/I[−] sample with a slight shift, again due to a changed polarizability of the environment. This indicates the absence of strong electronic coupling with significant influence on the absorption of the two compound materials.

For the photoluminescence from specific, selected spots of CdSe/I[−]/AE 1 samples, a periodic variation with time was reported in [12], which has been explained by energy transfer between CdSe QDs and AE molecules. To clarify whether indications for energy transfer can be globally found for the samples investigated in this paper, representative steady-state photoluminescence spectra are shown in figure 4(b). The CdSe/nat film shows strong and sharp emission centered around 629 nm while all other films exhibit much weaker photoluminescence [3]. In the CdSe/I[−] film nearly all

photoluminescence is quenched probably due to surface trap states, since no organic ligands are available to passivate the surface [3, 32, 33]. Only a very weak and broad photoluminescence from emissive trap states of the QDs is observed [3, 34]. The two AE films show very broad emission, again as a result of the different possible rotamers in the films [12, 31]. The two CdSe/I[−]/AE films show the most interesting results, since their spectra cannot be described as a superposition of the spectra of the CdSe/I[−] and AE films. At 641 nm a sharp peak is observed which can be attributed to slightly shifted QD emission. The reappearance of a distinct QD photoluminescence indicates that at least some of the QDs have well passivated surfaces, most likely due to bound AEs [33]. Hence, the native ligands, which have a wide HOMO-LUMO gap and electronically isolate the QDs, can be omitted without losing the QD photoluminescence. The use of CdSe/I[−] is thus beneficial as it increases the chances of energy or charge transfer. Beneath the sharp emission a broad emissive feature is apparent, which could either result from emission of the AEs or from unpassivated QDs. Taken together, the differences in the steady-state photoluminescence spectra of the samples investigated in this paper can be explained by differences in the passivation of the CdSe QDs without the need to involve energy transfer processes. Additional details to the photoluminescence results can be found in the supporting information.

The steady-state optical properties provide the basis for time-resolved transient absorption spectroscopy measurements to investigate the photophysics of the organic-inorganic hybrid systems with respect to energy or charge transfer. Pumping at a wavelength of 620 nm, hence at the band-edge of the QDs, leads to a strong signal in the QD-containing samples that does not show any spectral evolution and is therefore presented by a single spectrum and timetrace in figures 5(a), (b). The CdSe/nat and CdSe/I[−] films show similar, slightly shifted TA spectra consistent with the shift in the steady-state absorption. They exhibit the well-known features of CdSe QD TA spectra consisting of bleaches around 620 nm and 515 nm due to filling of the 1S(e) state and positive and negative features around 565 nm, 470 nm and 530 nm due to biexciton and Stark effects [29, 30, 35, 36]. The spectra of the two CdSe/I[−]/AE films resemble the spectra of the neat CdSe QD samples very closely, and no impact of the AEs is observed. However, in the dynamics, large differences are obtained, with a continuous decrease in the excited state lifetime going from the CdSe/nat sample to the CdSe/I[−] sample, with the two CdSe/I[−]/AE samples in between. The decays are multi-exponential which was attributed before to a differing number and type of trap states due to differences in the passivation of surface states of different QDs in the sample [29]. The neat AE films do not show a TA signal at this excitation wavelength since they only absorb at shorter wavelengths.

To clarify the impact of excited AEs on the photophysics of the CdSe/I[−]/AE films, further TA measurements with an excitation wavelength of 350 nm were performed. The obtained TA spectra at small delay times are shown in figure 5(c) and full two-dimensional TA maps can be found in

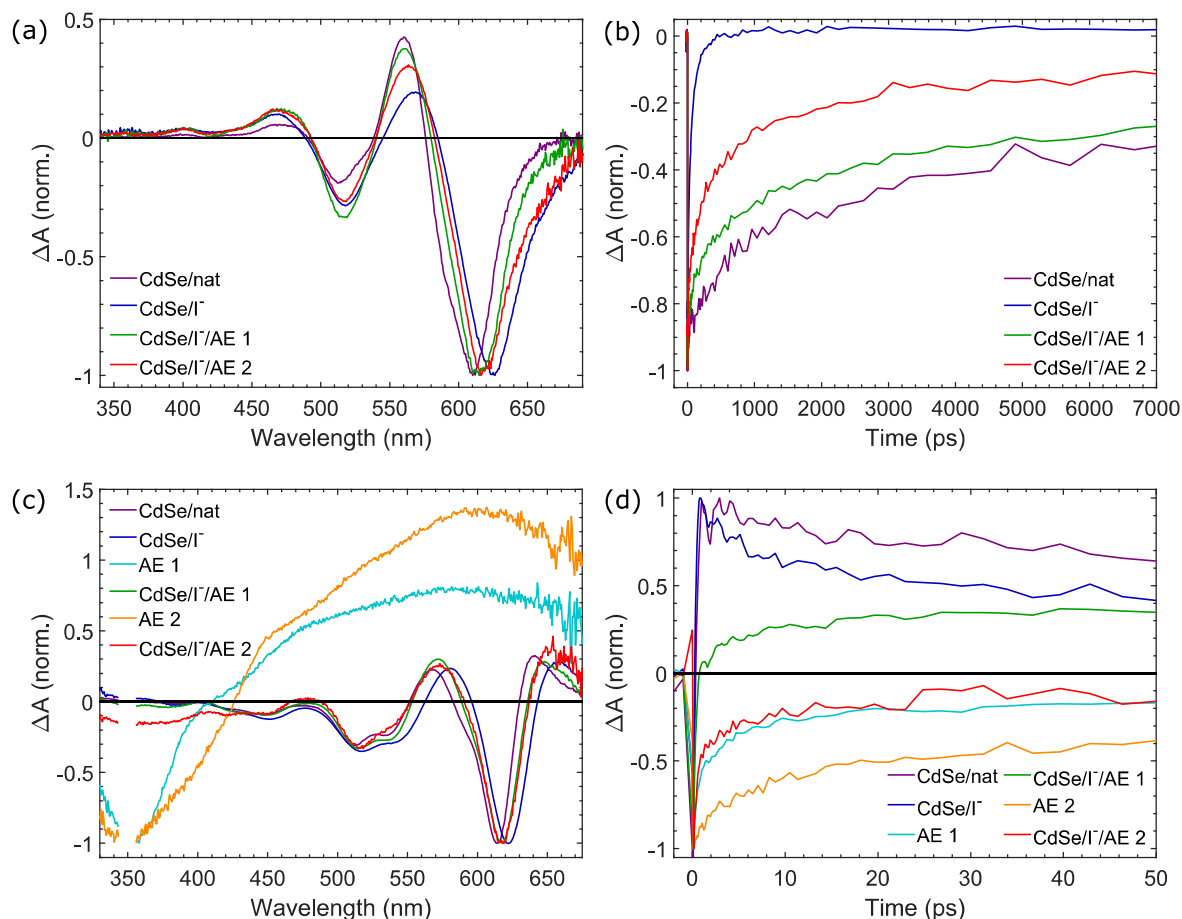


Figure 5. (a) TA spectra of the CdSe and CdSe/I⁻/AE films excited at 620 nm and time-integrated from 1 ps to 10 ps. (b) Timetraces of the spectra shown in (a) integrated from 511 nm to 521 nm. (c) TA spectra of the CdSe, AE and CdSe/I⁻/AE films excited at 350 nm and time-integrated from 0.1 ps to 0.5 ps. The region around 350 nm is left blank due to scattered laser light. (d) Timetraces of the spectra shown in (c) integrated from 355 nm to 385 nm, hence at the bleach of the AEs.

the supporting information. The TA spectra of the CdSe/nat and CdSe/I⁻ films show new, short-lived features around 645 nm, 540 nm and 450 nm after 350 nm excitation, which can be assigned to electrons excited to higher electronic states that quickly relax towards the 1S(e) state [29]. At longer times, the spectra resemble the ones in figure 5(a). The spectra of the two neat AE samples show relatively little spectral evolution and a non-exponential decay. They exhibit a bleach around their steady-state absorption maximum at the pump wavelength and a very broad excited state absorption at longer wavelengths. We attribute the broad, unstructured shape to energetically different transitions in different rotamers present in the solid films. Turning to the spectra of the CdSe/I⁻/AE samples, a domination of the CdSe signal in the spectra is found. Only at short wavelengths, at the bleach of the AEs, a difference between the spectra of the CdSe/I⁻/AE samples and the spectra of the neat CdSe samples is visible, which is more pronounced in the spectrum of the CdSe/I⁻/AE 2 film. To provide an overview of the dynamics, timetraces integrated from 355 nm to 385 nm are shown in figure 5(d). The spectra of the CdSe/nat and CdSe/I⁻ samples show a weak positive signal in this region while the spectra of the two neat AE films have their bleach at these wavelengths. The dynamics and spectra of the two

CdSe/I⁻/AE films can be approximately described as a superposition of the spectra of the neat CdSe and neat AE samples.

4. Discussion

With the above described results a scenario for the organization and interaction of the organic and inorganic components in the films can be developed. From the GISAXS results a clear difference in the mean distance between adjacent CdSe QDs was obtained. For both CdSe/I⁻/AE films a gap of approximately 1 nm between neighboring QDs was found, which can be explained by incorporated AEs and shows the structural similarity of the two systems with AE 1 and AE 2. From the appearance of sharp QD photoluminescence in the CdSe/I⁻/AE films, in contrast to the CdSe/I⁻ films, a passivation of surface trap states can be deduced, suggesting a binding of the incorporated AEs in the solid film. To further analyze the binding, PMIRRAS spectra were presented and the peaks were assigned to characteristic group frequencies. The sharp peaks assigned to the aromatic ring stretching mode around 1520 cm⁻¹ and the tertiary amino C–N stretching mode around 1180 cm⁻¹ show no significant differences

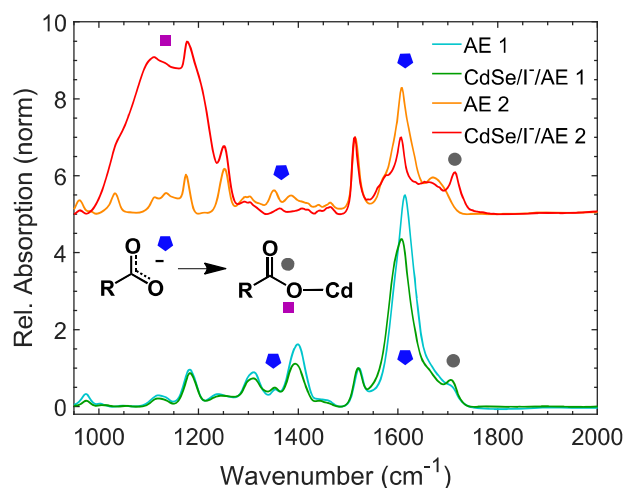


Figure 6. PMIRRAS spectra from figure 2 normalized at the aromatic ring stretching mode around 1522 cm^{-1} and offset along y-direction. The inset shows the proposed binding model and the peaks belonging to the characteristic group vibrations are marked by symbols.

between the neat AE samples and the CdSe/I[−]/AE films. Thus, the expectation that these groups are not directly involved in the binding is verified. The normalization of the PMIRRAS spectra of the AE and CdSe/I[−]/AE films at one of these peaks makes the changes of the intensity of the other peaks visible and quantifiable, as shown in figure 6. A clear decrease of the intensity of the vibrational peaks assigned to the carboxylate group in the CdSe/I[−]/AE 1 film compared to the neat AE 1 film is found and an increase of the intensity of the peak at 1707 cm^{-1} , which can be assigned to vibrations of a C=O group, but might also come from the CdSe/I[−] QDs. With the assumption that the peaks of the free carboxylate group disappear if the group is bound to a CdSe QD [23], the binding probability can be estimated. For the spectra of the AE 1 and CdSe/I[−]/AE 1 samples the area under the carboxylate peak at 1398 cm^{-1} was fitted since it has the least background beneath. A single Gaussian fit results in an intensity reduction of 31% for the spectrum of the CdSe/I[−]/AE 1 sample compared to the spectrum of the neat AE 1 film, indicating that on average more than two of the eight carboxylate groups per AE 1 molecule are bound to a QD.

The changes of the spectrum of the CdSe/I[−]/AE 2 sample compared to the spectrum of the neat AE 2 film are even more pronounced. The clear peak at 1714 cm^{-1} in the spectrum of the CdSe/I[−]/AE 2 sample, which is absent in the spectrum of the neat AE 2 film, is assigned to a C=O vibration. The peaks assigned to carboxylate vibrations almost disappeared and the very intense, broad peak around 1130 cm^{-1} is in a region where ether C–O stretch vibrations are located [18]. With these observations, the binding scheme of a monodentate interaction in figure 6 is suggested [37]. It can explain the weakening of the carboxylate vibrations, the appearance of a C=O vibration and the broad shape of the peak around 1130 cm^{-1} by differing binding geometries of the oxygen to a Cd surface atom. A clear quantification of the number of bound carboxylate groups per molecule is more

difficult for AE 2 since the peaks between 1300 cm^{-1} and 1400 cm^{-1} are less pronounced and around 1600 cm^{-1} several peaks overlap. A fit of the region from 1550 cm to 1750 cm (see Supporting Information) yields a reduction of the intensity that is not assigned to C=C and aromatic ring stretching mode vibrations of slightly more than 50%. Since in addition some background and other, weak vibrations are expected to contribute to the overall signal, on average at least two of the four carboxylate groups of one AE 2 molecule are bound to QDs. Due to the structure of the AE 2 molecule a connection of neighboring QDs by AE 2 molecules should be realized, consistent with the gap of $\sim 1\text{ nm}$ between neighboring QDs found by GISAXS. Based on the similar number of bound carboxylate groups per molecule and the similar distances between neighboring QDs in both CdSe/I[−]/AE systems, a connection of neighboring QDs by AE 1 seems likely, too.

Due to the binding of the AEs to the QDs, charge or energy transfer processes between the QDs and the AE molecules are likely, which we investigated by TA spectroscopy. The differences in the dynamics of the 1S(e) electron relaxation after band-edge excitation of the QDs at 620 nm can, however, simply be explained by the differences in surface trap passivation due to the ligands. The TA data of several samples and measurements with different excitation densities could be globally fitted with a parallel decay of two species. For the CdSe/I[−] films average decay times of 15 ps and 100 ps , for the CdSe/I[−]/AE 1 (CdSe/I[−]/AE 2) films average decay times of 250 ps (170 ps) and 7 ns (3 ns) and for the CdSe/nat films average decay times of 250 ps and 10 ns were found. The fraction of the signal that decayed with the nanosecond time constant is the largest for the CdSe/nat samples, followed by the CdSe/I[−]/AE 1 and CdSe/I[−]/AE 2 films. Taken together, the trap state passivation is the most effective for the native ligands, still relatively effective with AE 1 and less effective with AE 2. For the CdSe/I[−] sample no organic ligands are present, leading to a domination of trap state decay for all QDs in the film. The better passivation ability of AE 1 compared to AE 2 can be rationalized by twice the number of carboxylate groups on AE 1. No sign of an energy or electron transfer from the QDs to the AEs could be found, which would have resulted in a shortened 1S(e) electron signal lifetime. With 350 nm wavelength excitation, the TA spectra of the CdSe/nat, CdSe/I[−] and CdSe/I[−]/AE films show an intraband relaxation of the excited electron towards the 1S(e) state within 1.5 ps without significant differences between them. A unique fit of the time constants on longer timescales of the CdSe/I[−]/AE films was not possible since the CdSe QD signal as well as the AE signal already show non-exponential decays and the QD relaxation dynamics are additionally influenced by the number of surface trap states. Furthermore, the AE signal is weak compared to the QD signal and does not show sharp features due to the different rotamers. However, since the signal of the CdSe/I[−]/AE films can be approximately described as a superposition of the CdSe signal and the AE signal, also at 350 nm excitation no indication for charge or energy transfer was found. The absence of charge or energy transfer could possibly be due to

an unfavorable energy level alignment of the QDs and the AEs. The electrons and holes excited on the QDs could be confined to the QDs and energy transfer between different rotamers of the AEs could out-compete energy or charge transfer to the QDs, maybe due to a lack of frontier orbital overlap or an unfavorable orientation. An exact calculation or measurement of the energy levels in the solid thin film is, however, very difficult due to the different, fixed geometries of the AEs which result in strongly modified energetics of the different rotamers as visible from the absorption and emission spectra of the neat AE films.

5. Conclusion

We have studied thin film hybrid organic–inorganic nanomaterials composed of CdSe quantum dots and two arylethynyls with different substitutions. With the combination of GISAXS and PMIRRAS measurements the short range organization of the systems was analyzed and a binding scenario was developed. A binding of several carboxy groups of each AE molecule to CdSe QDs is found, resulting in a connection of neighboring QDs. Despite the chemical binding, surprisingly no indications for charge or energy transfer between either of the two AEs to the QDs or vice versa could be found by TA spectroscopy. The apparent contradiction with respect to the before reported periodic fluorescence variations of CdSe/I[−]/AE 1 samples can be explained by the larger probe area of the TA measurements and the eschewal to choose specific areas of the sample. The dominating effect of changed QD excited-state lifetimes is explained by differences in the surface passivation due to the different ligands, and their high passivation and binding capabilities render the AEs in hybrid compounds with QDs promising candidates for opto-electronic devices. Furthermore, we showed not only that PMIRRAS is a powerful tool to investigate the chemical binding in these exemplary hybrid thin-film systems, but that it should be applicable to a large variety of coupled organic–inorganic nanostructures. We believe that this is an important step towards a detailed understanding of the organic–inorganic interface and the organization of the compounds in solid materials, which is of fundamental importance for their successful technical application in a sustainable internet of things.

Acknowledgments

The authors gratefully acknowledge funding by the German Research Foundation (DFG) through the projects BR4869/4-1, SCHR 700/20-2 and TE479/6-1. MR acknowledges financial support from the Heidelberg Graduate School of Fundamental Physics. DR acknowledges funding by the Max Planck School Matter To Life project.

ORCID iDs

Antonia Weber  <https://orcid.org/0000-0002-8575-7525>
 Debkumar Rana  <https://orcid.org/0000-0001-8165-3289>
 Uwe Bunz  <https://orcid.org/0000-0002-9369-5387>
 Marcus Scheele  <https://orcid.org/0000-0002-2704-3591>
 Petra Tegeder  <https://orcid.org/0000-0002-5071-9385>
 Frank Schreiber  <https://orcid.org/0000-0003-3659-6718>
 Katharina Broch  <https://orcid.org/0000-0002-9354-292X>

References

- [1] Forrest S R 2004 *Nature* **428** 911–8
- [2] Kampen T U 2010 *Low Molecular Weight Organic Semiconductors* (Weinheim: Wiley-VCH)
- [3] Bera D, Qian L, Tseng T K and Holloway P H 2010 *Materials* **3** 2260–345
- [4] Scheele M, Brütting W and Schreiber F 2015 *Phys. Chem. Chem. Phys.* **17** 97–111
- [5] Steiner A M, Lissel F, Fery A, Lauth J and Scheele M 2021 *Angew. Chem. Int. Ed.* **60** 1152–75
- [6] Voznyy O, Sutherland B R, Ip A H, Zhitomirsky D and Sargent E H 2017 *Nat. Rev. Mater.* **2** 1–10
- [7] Singhal P and Ghosh H N 2018 *J. Phys. Chem. C* **122** 17586–600
- [8] Mathias F, Fokina A, Landfester K, Tremel W, Schmid F, Char K and Zentel R 2015 *Macromol. Rapid Commun.* **36** 959–83
- [9] Wurst K M, Bender M, Lauth J, Maiti S, Chassé T, Meixner A, Siebbeles L D A, Bunz U H F, Braun K and Scheele M 2018 *Angew. Chem. Int. Ed.* **130** 11733–7
- [10] Wu M, Congreve D N, Wilson M W B, Jean J, Geva N, Welborn M, Van Voorhis T, Bulović V, Bawendi M G and Baldo M A 2016 *Nat. Photon.* **10** 31–4
- [11] Gray V, Allardice J R, Zhang Z and Rao A 2021 *Chem. Phys. Rev.* **2** 031305
- [12] Kumar K et al 2021 *ACS Nano* **15** 480–8
- [13] Thomas A, Nair P V and George Thomas K 2014 *J. Phys. Chem. C* **118** 3838–45
- [14] Sayevich V et al 2017 *ACS Nano* **11** 1559–71
- [15] Alagna N, Lustres J L P, Roozbeh A, Han J, Hahn S, Berger F J, Zaumseil J, Dreuw A, Bunz U H and Buckup T 2020 *J. Phys. Chem. B* **124** 9163–74
- [16] André A et al 2017 *Chem. Commun.* **53** 1700–3
- [17] Son J G, Choi E, Piao Y, Han S W and Lee T G 2016 *Nanoscale* **8** 4573–8
- [18] Coates J 2006 Interpretation of infrared spectra, a practical approach *Encyclopedia of Analytical Chemistry* (<https://doi.org/10.1002/9780470027318.a5606>)
- [19] Hipps K W and Crosby G A 1979 *J. Phys. Chem.* **83** 555–562
- [20] Buffeteau T, Desbat B and Turlet J M 1991 *Appl. Spectrosc.* **45** 380–9
- [21] Young A G, Al-Salim N, Green D P and McQuillan A J 2008 *Langmuir* **24** 3841–9
- [22] SpectraBase n-methylformamide transmission infrared spectrum, spectrum ID 3LquiOAHvGS, John Wiley & Sons, Inc (<https://spectrabase.com/spectrum/3LquiOAHvGS>) (Accessed: 28 October, 2021)
- [23] Kaposov A Y, Cardolaccia T, Albert V, Badaeva E, Kilina S, Meyer T J, Tretiak S and Sykora M 2011 *Langmuir* **27** 8377–83
- [24] Maiti S, Maiti S, Khan A H, Wolf A, Dorfs D, Moreels I, Schreiber F and Scheele M 2019 *Chem. Mater.* **31** 2443–9
- [25] Zaluzhnyy I A et al 2017 *Nano Lett.* **17** 3511–7

- [26] Zaluzhnyy I A, Kurta R P, Scheele M, Schreiber F, Ostrovskii B I and Vartanyants I A 2019 *Materials* **12** 3464
- [27] Lee B, Podsiadlo P, Rupich S, Talapin D V, Rajh T and Shevchenko E V 2009 *J. Am. Chem. Soc.* **131** 16386–8
- [28] Ekimov A I, Hache F, Schanne-Klein M C, Ricard D, Flytzanis C, Kudryavtsev I A, Yazeva T, Rodina A V and Efros A L 1993 *JOSA B* **10** 100–7
- [29] Klimov V I, McBranch D W, Leatherdale C A and Bawendi M G 1999 *Phys. Rev. B* **60** 13740
- [30] Zhang C, Do T N, Ong X, Chan Y and Tan H S 2016 *Chem. Phys.* **481** 157–64
- [31] Wilson J N, Smith M D, Enkelmann V and Bunz U H 2004 *Chem. Commun.* **15** 1700–1
- [32] Wuister S F, de Mello Donega C and Meijerink A 2004 *J. Phys. Chem. B* **108** 17393–7
- [33] Gao Y and Peng X 2015 *J. Am. Chem. Soc.* **137** 4230–5
- [34] Nirmal M, Norris D J, Kuno M, Bawendi M G, Efros A L and Rosen M 1995 *Phys. Rev. Lett.* **75** 3728
- [35] Klimov V, Hunsche S and Kurz H 1994 *Phys. Rev. B* **50** 8110
- [36] Norris D J, Sacra A, Murray C B and Bawendi M G 1994 *Phys. Rev. Lett.* **72** 2612
- [37] Fritzinger B, Capek R K, Lambert K, Martins J C and Hens Z 2010 *J. Am. Chem. Soc.* **132** 10195–201